

Modulation of Australian Precipitation by Meridional Gradients in East Indian Ocean Sea Surface Temperature

CAROLINE C. UMMENHOFER, ALEXANDER SEN GUPTA, ANDRÉA S. TASCHETTO,
AND MATTHEW H. ENGLAND

Climate Change Research Centre, University of New South Wales, Sydney, New South Wales, Australia

(Manuscript received 7 January 2009, in final form 1 June 2009)

ABSTRACT

This study explores the impact of meridional sea surface temperature (SST) gradients across the eastern Indian Ocean on interannual variations in Australian precipitation. Atmospheric general circulation model (AGCM) experiments are conducted in which the sign and magnitude of eastern Indian Ocean SST gradients are perturbed. This results in significant rainfall changes for western and southeastern Australia. A reduction (increase) in the meridional SST gradient drives a corresponding response in the atmospheric thickness gradients and results in anomalous dry (wet) conditions over Australia. During simulated wet years, this seems to be due to westerly anomalies in the thermal wind over Australia and anomalous onshore moisture advection, with a suggestion that the opposite occurs during dry conditions. Thus, an asymmetry is seen in the magnitude of the forced circulation and precipitation response between the dry and wet simulations. To assess the relative contribution of the SST anomalies making up the meridional gradient, the SST pattern is decomposed into its constituent “poles,” that is, the eastern tropical pole off the northwest shelf of Australia versus the southern pole in the central subtropical Indian Ocean. Overall, the simulated Australian rainfall response is linear with regard to the sign and magnitude of the eastern Indian Ocean SST gradient. The tropical eastern pole has a larger impact on the atmospheric circulation and Australian precipitation changes relative to the southern subtropical pole. However, there is clear evidence of the importance of the southern pole in enhancing the Australian rainfall response, when occurring in conjunction with but of opposite sign to the eastern tropical pole. The observed relationship between the meridional SST gradient in the eastern Indian Ocean and rainfall over western and southeastern Australia is also analyzed for the period 1970–2005. The observed relationship is found to be consistent with the AGCM results.

1. Introduction

Variations in upper Indian Ocean properties have been implicated in widespread changes to precipitation over adjacent landmasses (Saji and Yamagata 2003), including East Africa (e.g., Webster et al. 1999; Black et al. 2003; Hastenrath 2007), India, Indonesia (D’Arrigo and Wilson 2008), and Australia (Ashok et al. 2003; England et al. 2006; Ummenhofer et al. 2008). Recently, non-uniform warming trends in the Indian Ocean have been described (Alory et al. 2007; Ihara et al. 2008) and there are indications that characteristics of the dominant mode of tropical Indian Ocean variability may be changing (Abram et al. 2008). As such, there is a pressing need

for a better understanding of the mechanisms by which Indian Ocean variability modulates regional rainfall, particularly in the context of improved seasonal rainfall forecasting. The extended persistence of temperature anomalies in the ocean, in contrast to the higher-frequency variability in the atmosphere, in conjunction with a more thorough understanding of the links between Indian Ocean sea surface temperature (SST) and regional climate, can help improve seasonal rainfall predictions and thus, ultimately, water and agricultural management.

This study follows previous work linking a characteristic pattern of Indian Ocean SST anomalies, and an associated reorganization of the basinwide atmospheric circulation, to Australian rainfall anomalies in observations and climate model experiments (England et al. 2006; Ummenhofer et al. 2008). The SST pattern (Fig. 1) exhibits features of both the tropical and subtropical Indian Ocean dipoles, but is distinct from previous

Corresponding author address: Caroline Ummenhofer, Climate Change Research Centre, University of New South Wales, Sydney, NSW 2052, Australia.
E-mail: c.ummenhofer@unsw.edu.au

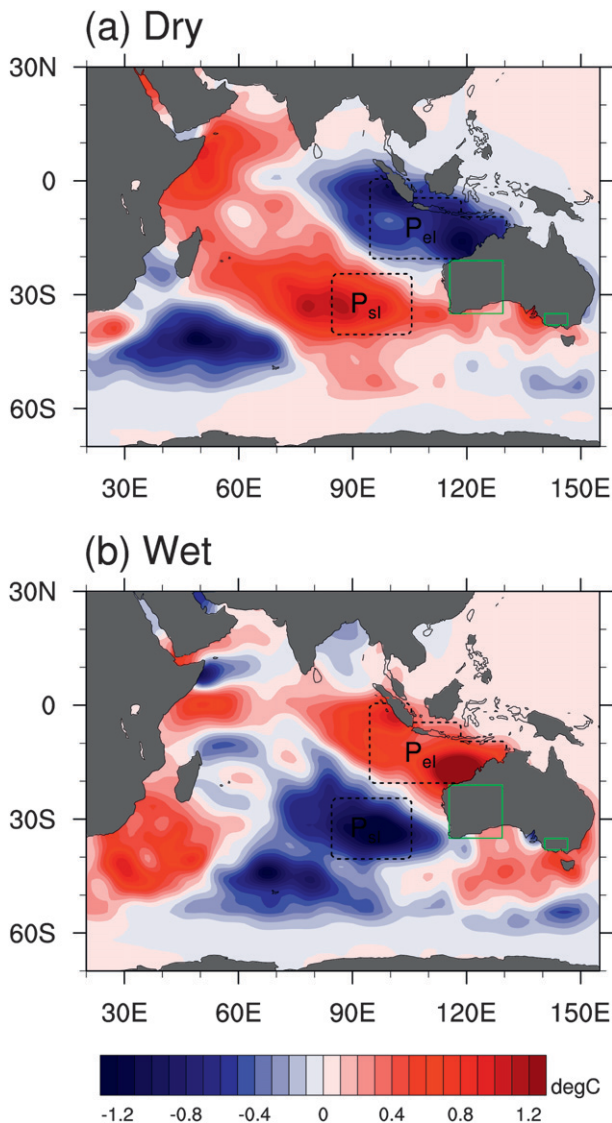


FIG. 1. Average May–September SST anomaly (in $^{\circ}\text{C}$) for the (a) dry and (b) wet cases, superimposed as a perturbation on the climatological SST across the Indian Ocean for individual poles, separately and in combination, with the poles indicated by the dashed black boxes as P_{el} and P_{sl} . The green boxed areas in (a),(b) denote the WA and SEA regions analyzed in this study. The full seasonal evolution of the SST perturbations employed in the experiments in this study is shown in Fig. 1 of Ummenhofer et al. (2008).

descriptions of the tropical Indian Ocean dipole (IOD; Saji et al. 1999; Webster et al. 1999) and the subtropical Indian Ocean dipole (SIOD; Behera and Yamagata 2001). In particular, the pattern of SST anomalies shows a tripolar structure across the Indian Ocean: one pole located in the tropical eastern Indian Ocean off the northwest shelf of Australia, a region of opposite sign to the south in the central subtropical Indian Ocean, and a third pole to the south of Madagascar in the southwest

Indian Ocean. In atmospheric general circulation model (AGCM) experiments, Ummenhofer et al. (2008) assess the effect of this basinwide anomalous SST pattern on Australian rainfall. They find anomalous dry (wet) conditions across western regions of Australia linked to a reduced (enhanced) thickness gradient across the eastern Indian Ocean induced by positive (negative) phases of the tripole pattern. This results in easterly (westerly) anomalies in the thermal wind and anomalous offshore (onshore) moisture flux onto the continent accounting for significant shifts in rainfall over Western Australia (WA) and southwest Western Australia (SWWA).

Meridional SST gradients across the eastern Indian Ocean seem to be a key factor for the Australian rainfall response (Ummenhofer et al. 2008). Especially across the eastern half of the Indian Ocean, the distribution of SST anomalies described here is reminiscent of the observed pattern described by Nicholls (1989), who also linked these SST anomalies to variations in Australian winter rainfall. When investigating Australian rainfall patterns, Drosowsky (1993b) found links between such Indian Ocean SST in dry (wet) winters and anomalous high (low) pressure over southern Australia with ridges (troughs) extending northwest into the Indian Ocean. Furthermore, Drosowsky and Chambers (2001) showed improved skill of rainfall hindcasts over southeast Australia (SEA) when using a similar SST pattern as a predictor in addition to using the Southern Oscillation index. Frederiksen et al. (1999) found that the observed SST gradient between the Indonesian Archipelago and the central Indian Ocean affects winter precipitation over WA and SEA. These are the two regions in Australia that will also form the major focus of this study.

In AGCM experiments, Frederiksen and Balgovind (1994) explored the effect of an enhanced gradient in SST anomalies between the Indonesian Archipelago and the central Indian Ocean on synoptic events that were conducive to Australian winter rainfall. They showed strong cross-equatorial flow northwest of Australia interacting with short-wave midlatitude disturbances accounting for enhanced rainfall. They further suggested that the magnitude of the Australian rainfall response is more sensitive to the strength of the meridional gradient than its exact location, and that the SST anomalies in the Indonesian region affect the rainfall anomalies disproportionately highly. It is therefore of interest to investigate these questions in regard to the role and mechanism of the meridional SST gradient in the east Indian Ocean for Australian rainfall using AGCM experiments.

Precipitation across Australia has sustained considerable trends over the last few decades. Especially prominent is a decline in austral winter rainfall in SWWA

(IOCI 2002, and references therein) and autumn–winter rainfall over SEA (Murphy and Timbal 2008, and references therein). Both these regions provide a large proportion of Australia’s agricultural production, which relies heavily on the predominant cool season rainfall. A sudden decrease in SWWA winter precipitation in the 1970s has been associated with changes in large-scale mean sea level pressure (Allan and Haylock 1993), the southern annular mode (SAM; Cai and Cowan 2006; Hendon et al. 2007), shifts in synoptic systems (Hope 2006; Frederiksen and Frederiksen 2007), land cover changes (Pitman et al. 2004; Timbal and Arblaster 2006), anthropogenic forcing (Timbal et al. 2006; Cai and Cowan 2006), and natural multidecadal variability (Cai et al. 2005), with a combination of several factors most likely. For SEA, the drying has been especially pronounced over the Murray–Darling Basin, with rainfall reductions translating to river system inflows for 2001–05 of only 40% of the long-term mean (Murphy and Timbal 2008). Murphy and Timbal (2008) suggested that large-scale changes in the SAM and the position of the subtropical ridge play a role in the reduced number and impact of rain-bearing systems during autumn for SEA. Cai and Cowan (2008) linked the decrease in late autumn rainfall to the less frequent occurrence of La Niña events since 1950. Ummenhofer et al. (2009a) associated both the recent drought and many of the large historical droughts over SEA with a conspicuous absence of negative IOD events. A lack of negative IOD events deprives the region of its normal rainfall quota. This further suggests some influence of the long-term Indian Ocean SST changes on Australian precipitation trends.

With the Indian Ocean exhibiting spatially non-uniform warming trends, changes in the characteristics of SST patterns conducive to Australian rainfall might occur. The observed subsurface cooling in the eastern tropical Indian Ocean due to a shoaling of the thermocline (Alory et al. 2007) makes this region more sensitive to the wind–thermocline feedback and therefore predisposes the Indian Ocean to more positive IOD events (Ihara et al. 2008) over recent decades. On longer time scales, Abram et al. (2008) also found an intensification of tropical Indian Ocean variability with more intense and frequent positive IOD events during the twentieth century. Positive IOD events generally coincide with below-average winter rainfall across southern and western regions of Australia (Ashok et al. 2003; Ummenhofer et al. 2009a). England et al. (2006) suggested that recent Indian Ocean warming trends across the eastern basin bias the SST distribution to a pattern that corresponds to anomalous dry conditions for SWWA. Furthermore, these nonuniform trends in Indian Ocean surface properties result in changed meridional SST gradients across

the eastern Indian Ocean. In light of these changes, and their projected continuation (Vecchi and Soden 2007), an improved understanding of the role that meridional SST gradients play for Australian rainfall on interannual time scales is desirable. Furthermore, the observed drying trends across southern regions of Australia have motivated previous work (e.g., England et al. 2006; Ummenhofer et al. 2008, and references therein) in an attempt to better understand the role that Indian Ocean variability plays on interannual time scales under these exacerbated conditions. We thus complement previous work by investigating links between winter season rainfall across WA/SEA and meridional gradients in east Indian Ocean SST.

The remainder of the paper is structured as follows: in section 2, the climate model, experimental setup, and datasets are described. The next section describes the rainfall distribution in the AGCM experiments (section 3a), as well as its dependence on the SST gradient across the eastern Indian Ocean (section 3b). In section 4 we explore the mechanisms driving the precipitation patterns by assessing changes to the large-scale atmospheric circulation in the experiments. Results from the AGCM experiments are linked to observational evidence in section 5. Section 6 summarizes the findings.

2. Model and datasets

a. Climate model

The climate model used for the experiments is the National Center for Atmospheric Research (NCAR) Community Climate System Model, version 3 (CCSM3; Collins et al. 2006), run in the atmosphere-only configuration. The atmospheric component of CCSM3, the Community Atmosphere Model (CAM3), uses a spectral dynamical core, a T42 horizontal resolution (approximately 2.8° latitude/longitude), and 26 vertical levels. The CCSM3 model, its components, and configurations are described in Collins et al. (2006), and more specifically the atmospheric component CAM3 by Hurrell et al. (2006). Several studies assess the model’s performance and suitability for applications in climate research relevant for the present study, in particular in regard to the representation of the hydrological cycle (Hack et al. 2006), tropical Pacific climate variability (Deser et al. 2006), variability associated with the El Niño–Southern Oscillation (ENSO; Zelle et al. 2005), and monsoon regimes (Meehl et al. 2006). Several biases in the model have been documented, most notably associated with tropical Pacific climate (i.e., the intertropical convergence zone, South Pacific convergence zone; e.g., Zhang and Wang 2006), and ENSO spatial and temporal variability (e.g., Deser et al. 2006). These issues and their relevance

for the Indian Ocean region have been explored by Ummenhofer et al. (2008, 2009b).

The model reproduces the spatial patterns of Australian precipitation with wetter coastal regions along the northern and eastern coastline and a very dry interior, though the contrast is weaker than in observations (Ummenhofer et al. 2008). The precipitation regimes across the continent varying with the seasonal cycle (i.e., summer monsoonal rainfall in the north, winter rainfall in the south) compare very favorably with observations. For more details see Ummenhofer et al. (2008).

b. Experimental setup

A detailed description of the experimental setup is given in Ummenhofer et al. (2008, 2009b). The AGCM experiments are forced by the monthly Hurrell SST climatology (Hurrell et al. 2006, 2008), which is based on Reynolds SST (Smith and Reynolds 2003, 2004) and Hadley anomalies (Rayner et al. 2003). A set of 80 ensemble members, each run for one year starting on 1 January with this SST climatology, represents the control run (CNTRL). In the perturbation runs, we superimposed an SST anomaly pattern across the Indian Ocean. To account for any long-term variability in the SST forcing, perturbation runs were started from a variety of years spanning the control run and integrated from the start of January for one year. The ensemble included 60 positive and 60 negative 1-yr integrations. The SST anomalies in the perturbation runs were derived from composites of observed average monthly SST anomalies for years defined as being extremely dry or wet over SWWA by England et al. (2006). The composite SST anomalies of England et al. (2006) were scaled by a factor of 3 to account for inherent internal variability in the atmosphere. As detailed by Ummenhofer et al. (2008), this scaling does not mean that the SST anomaly pattern is unrealistic, but makes the anomalies in the perturbation experiments comparable in magnitude to the values observed in a particular *extreme* year (e.g., 2006). The full seasonally evolving SST perturbation pattern employed in the AGCM experiments here is shown in Fig. 1 of Ummenhofer et al. (2008). This characteristic pattern of Indian Ocean SST anomalies first appears around May, is fully formed by July, and decays in late austral spring (England et al. 2006; Ummenhofer et al. 2008). It features components of both a tropical IOD and an SIOD signal. This pattern closely resembles a dominant mode of variability in the Indian Ocean (Santoso 2005), and previous work has explored certain components of these characteristic SST features in the tropical (e.g., Saji et al. 1999; Webster et al. 1999) and the subtropical Indian Ocean (e.g., Behera and Yamagata 2001; Reason 2002), as well as links between the SST anomalies across the

eastern Indian Ocean and regional rainfall (Nicholls 1989; Frederiksen and Balgovind 1994; England et al. 2006; Ummenhofer et al. 2008). For the period 1970–2003, the pattern explains about 16% of the overall observed SST variability across the Indian Ocean and has a dominant frequency of ~ 8 yr (Santoso 2005). This is similar to the recurrence frequency of ~ 6 – 7 yr in the composites described by England et al. (2006) in observations and a natural-variability (unforced) multicentury climate model simulation. For comparison, the IOD explains about 12% of the total observed tropical Indian Ocean SST variability (Saji et al. 1999).

Additional experiments, detailed below, are also carried out using various regional subsets of the poles evident in the full pattern of Fig. 1, which shows the average May–September SST anomalies used in the perturbation runs for both the dry and wet ensemble set. A set of 60 one-year ensemble runs (with slightly different initial conditions) is carried out for each of the perturbation fields applied. The entire anomalous SST pattern shown in Fig. 1 over the Indian Ocean region is termed P_i . To assess the importance of local SST anomalies (or poles) in modulating regional rainfall, and to quantify their separate contributions, perturbation experiments are also conducted with individual poles or a subset of the poles: namely P_{ei} with the eastern tropical pole only (centered at 10°S , 110°E), P_{si} with the subtropical pole only (centered at 30°S , 95°E), and P_{ei+si} with both the eastern and southern poles. The locations of the poles used in the different experiments are indicated as dashed boxes in Fig. 1. To reduce spurious atmospheric circulation set up by unrealistic gradients at the “edges” of the poles, smoothing has been applied with a tapering of SST anomalies over a 10° latitude/longitude range.

c. Climatological data

Results from the AGCM simulations are compared to observations. For the period 1970–2005, we use monthly data for observed Australian precipitation from the Australian Bureau of Meteorology (Lavery et al. 1997). It provides high-quality historical precipitation observations over Australia at 0.5° latitude/longitude resolution. The SST data are based on the Hadley Centre Sea Ice and SST dataset (HadISST) product with 1° latitude/longitude resolution provided by the Met Office (Rayner et al. 2003).

3. Australian precipitation response

a. Precipitation changes

To assess the effect that the SST anomalies in the different experiments have on Australian climate, we present spatial maps of rainfall anomalies during the austral winter season (i.e., for the May–September months; Fig. 2),

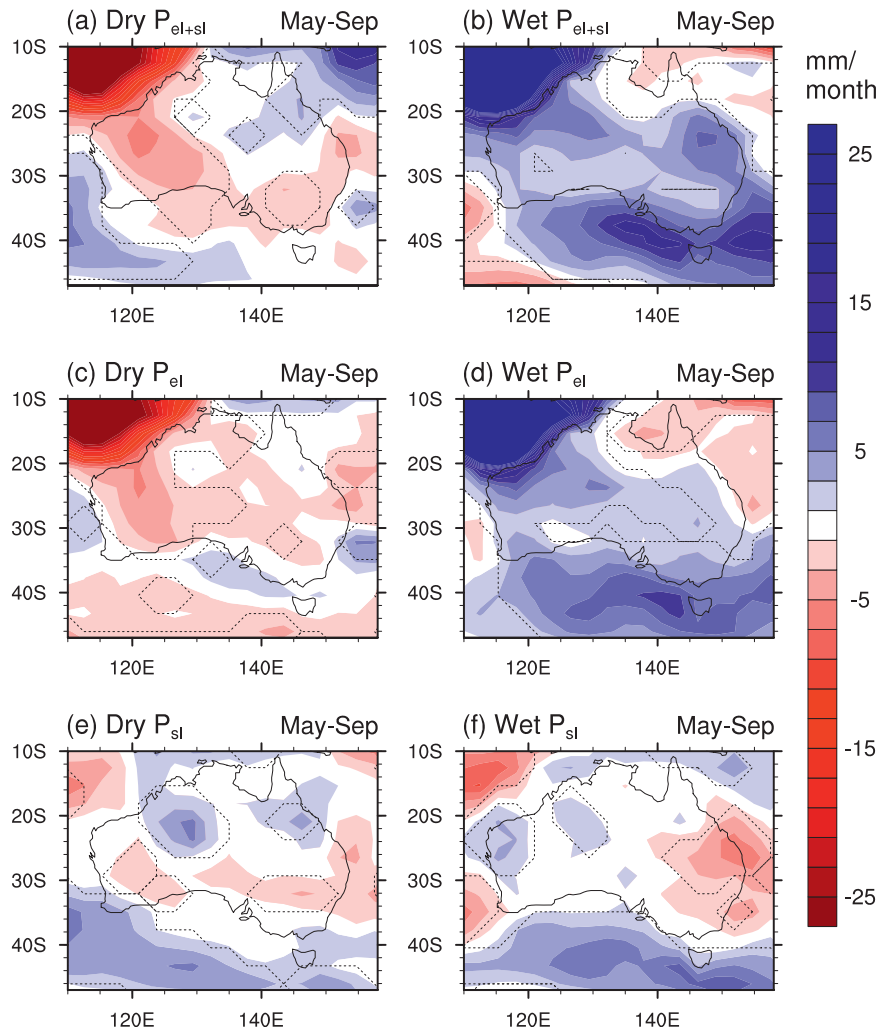


FIG. 2. Precipitation anomalies (in mm month^{-1}) for the (left) dry and (right) wet cases, respectively, for (a),(b) P_{el+sl} , (c),(d) P_{el} , and (e),(f) P_{sl} , averaged over the May–September months. The area enclosed by the dashed contours denotes anomalies that are significant at the 90% confidence level as estimated by a two-tailed t test.

when the majority of rainfall occurs across southern regions of Australia (Drosowsky 1993a). To determine the significance of the spatial anomaly fields, a two-tailed t test is used. This test estimates the statistical significance at which the anomalies in the perturbed experiment are distinguishable from the CNTRL at each grid point. The same technique is applied to all spatial anomaly fields throughout the study (e.g., Figs. 6–8).

In the AGCM simulations, marked differences in winter precipitation are seen across the Australian continent between the dry and wet cases (Fig. 2). In the dry cases, significantly below-average rainfall is recorded over much of WA in both the P_{el+sl} and P_{el} experiments (Figs. 2a–d). In contrast, the spatial extent of anomalous dry (wet) conditions is very much reduced when forced by the subtropical pole on its own

(P_{sl} ; Figs. 2e,f). Overall, the subtropical pole on its own does not seem to affect Australian precipitation in any significant way, the exception being a slight increase in the dry P_{sl} case over SWWA in line with earlier results by Ummenhofer et al. (2008). For SEA, the rainfall response is strengthened, however, when a subtropical SST anomaly, of opposite sign to the eastern tropical pole, is also present. We find that the spatial extent and magnitude of the rainfall anomalies over SEA are enhanced in the P_{el+sl} ensemble set (Figs. 2a,b) relative to the P_{el} cases (Figs. 2c,d). This result provides a first indication of the importance of the meridional SST gradient across the eastern Indian Ocean for SEA rainfall.

Changes in rainfall distribution across Australia are further investigated, with a focus on two regions: Western Australia, delimited by 21°–35°S, 115°–129°E

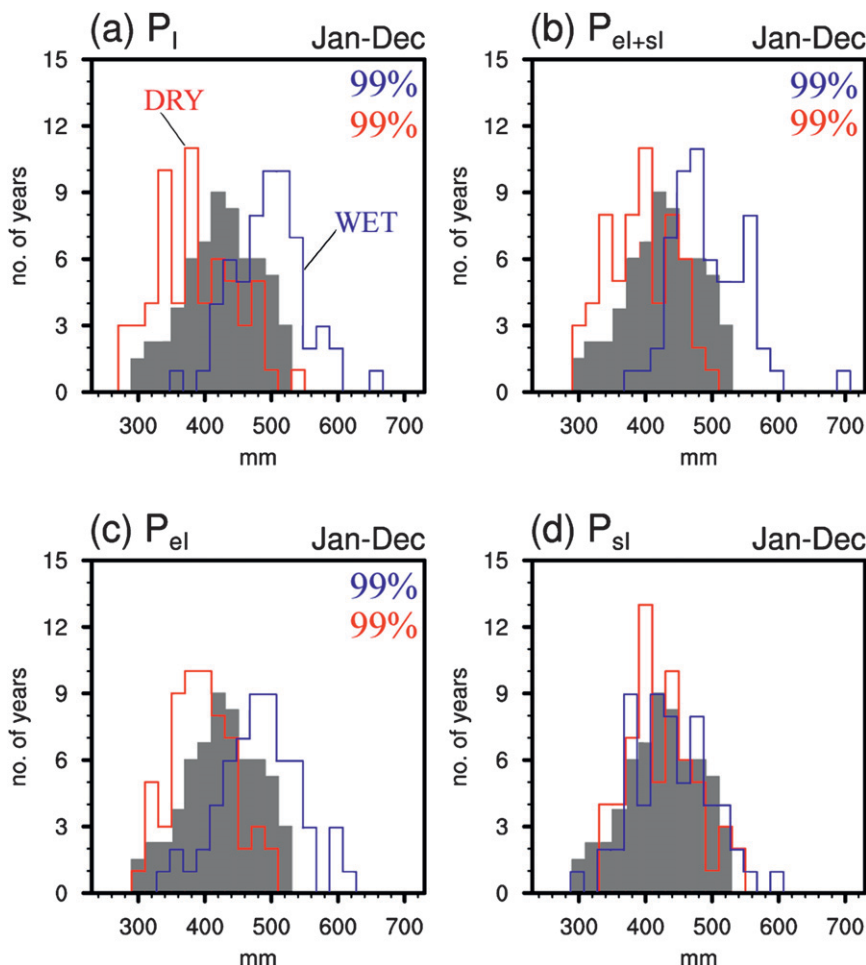


FIG. 3. Frequency distribution of annual precipitation spatially averaged across WA (sub-region indicated in Fig. 1): annual rainfall amount (in mm) for the following experiments: (a) P_I , (b) P_{el+sl} , (c) P_{el} , and (d) P_{sl} . The shaded gray rainfall distribution represents the CNTRL (normalized to the number of ensemble members in the perturbed cases), while the dry (wet) perturbed cases are indicated with red (blue) outlines. Significance levels above 80%, as determined by a Mann–Whitney test, are indicated at the top right.

(see box in Fig. 1), and southeast Australia, covering the area 35° – 38° S, 141° – 146° E (see box in Fig. 1). The non-parametric Mann–Whitney rank test (von Storch and Zwiers 1999) is used to determine the significance level at which the rainfall frequency distribution in a particular region (WA and SEA) in the various experiments differs from the CNTRL.

In the AGCM experiments, the annual mean precipitation, spatially averaged across WA, is $426 \pm 56 \text{ mm yr}^{-1}$ in the CNTRL, while it is $387 \pm 60 \text{ mm yr}^{-1}$ in the dry and $481 \pm 55 \text{ mm yr}^{-1}$ in the wet case when using the SST anomalies across the entire Indian Ocean (Fig. 3a). The shifts in precipitation for the perturbed cases are especially prominent at the upper and lower end of the distribution. For example, in the CNTRL set 31% of years receive less than 400 mm yr^{-1} , while this

occurs for 58% in the dry and only 5% of years in the wet case. Less than 300 mm yr^{-1} is received for only 1% of years in the CNTRL, but 5% for the dry case. At the upper end of the distribution, more than 500 mm yr^{-1} occurs for only 3% of years in the dry case, 10% in the CNTRL, but 38% in the wet case. In none of the years in either the CNTRL or dry case is more than 550 mm yr^{-1} annual precipitation recorded, while 12% of years in the wet case receive this amount.

When investigating the other experiments with individual and combined poles across the eastern Indian Ocean, we see a similar pattern emerging for the rainfall distribution. Both the P_{el+sl} and P_{el} show a comparable shift in rainfall relative to the CNTRL toward the upper (lower) end of the distribution for the wet (dry) cases (Figs. 3b,c). The mean rainfall in the P_{el+sl} case for the

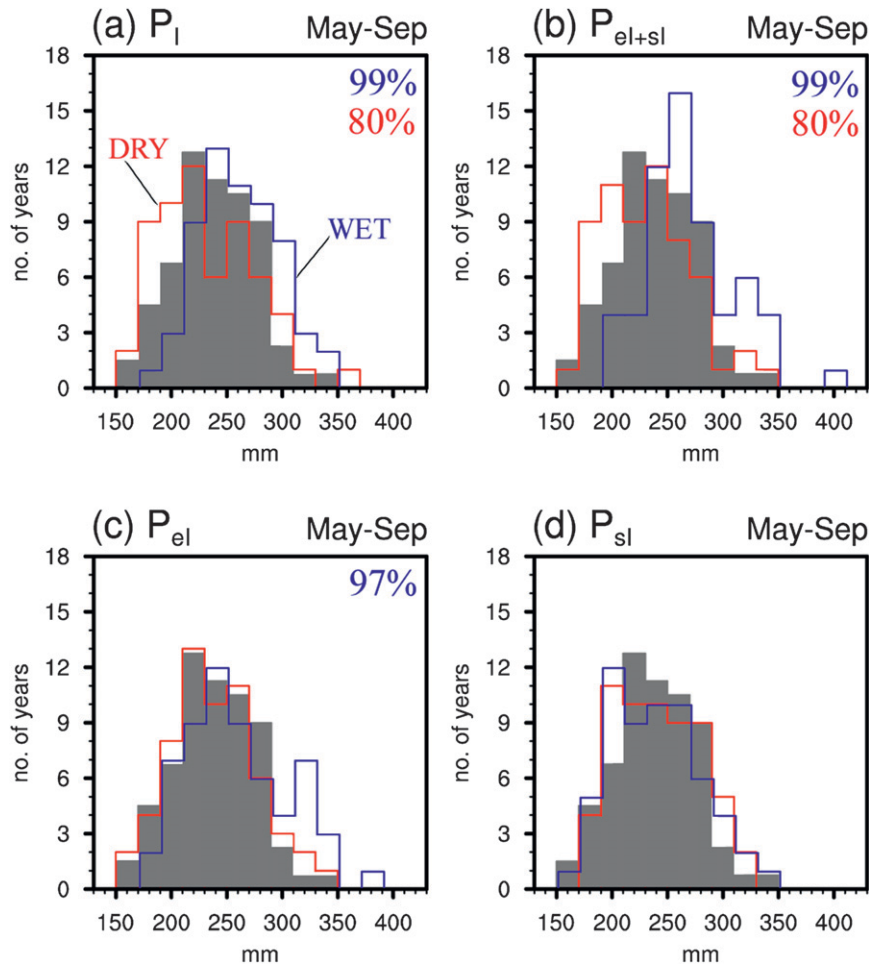


FIG. 4. Frequency distribution of precipitation spatially averaged across SEA (subregion indicated in Fig. 1): rainfall amount (in mm) summed over the May–September months for the following experiments: (a) P_I , (b) P_{el+sl} , (c) P_{el} , and (d) P_{sl} . The shaded gray rainfall distribution represents the CNTRL (normalized to the number of ensemble members in the perturbed cases), while the dry (wet) perturbed cases are indicated with red (blue) outlines. Significance levels above 80%, as determined by a Mann–Whitney test, are indicated at the top right.

dry (394 mm yr^{-1}) and wet (478 mm yr^{-1}) scenarios is slightly more extreme than for the P_{el} case (397 and 463 mm yr^{-1} , respectively). In contrast, the southern pole on its own (P_{sl}) does not drive a significant shift in the rainfall distribution across WA (Fig. 3d). These results indicate that the majority of the precipitation response over WA in the AGCM experiments can be attributed to the SST anomalies in the eastern pole. However, there seems to be an indication that precipitation anomalies are enhanced, albeit not significantly, when an anomaly of the opposite sign is also present in the subtropical Indian Ocean (i.e., the P_{el+sl} case). This is in agreement with the findings of Frederiksen and Balgovind (1994) for a wet case scenario.

An investigation of changes in precipitation for SEA for the May–September months is also undertaken,

when the majority of rainfall is received over the southeast region. In the AGCM experiments, SEA records a mean precipitation of $239 \pm 37 \text{ mm}$ integrated over the May–September months for the CNTRL, $231 \pm 42 \text{ mm}$ for the dry, and $260 \pm 35 \text{ mm}$ for the wet case when using the full SST anomaly pattern (Fig. 4a). Despite the region’s remoteness from the area of the perturbation, the resulting shifts in the rainfall are significant (at the 99% level) for the wet cases. Changes are especially apparent at the extreme ends of the distribution: only 2% of wet years receive less than 200 mm of precipitation, while this occurs for 14% of years in the CNTRL and 27% in the dry case. More than 300 mm is recorded for 17% of the years in the wet case, but only 4% and 7% in the CNTRL and dry case, respectively.

In the P_{el+sl} case, similar shifts in the precipitation are seen for SEA (Fig. 4b), significant at the 99% level for both the dry and wet cases. However, when using SST anomalies in the eastern pole on its own, a significant change relative to the CNTRL is only seen for the wet case (Fig. 4c). Our experiments thus suggest that for SEA precipitation the eastern pole on its own exhibits less of an impact unless it occurs in conjunction with the southern pole of opposite sign. In fact, for the wet cases, the rainfall distribution in P_{el+sl} and P_{el} is significantly different (at the 80% level). As for WA, the southern pole on its own does not cause a significant rainfall response for SEA (Fig. 4d), despite playing an important role in the net Indian Ocean response. Earlier work by Frederiksen and Balgovind (1994) raised the possibility that Australian rainfall is fairly insensitive to the SST anomalies in the central Indian Ocean relative to the Indonesian region.

b. Relation to SST gradients

As suggested in previous work (e.g., Nicholls 1989; Frederiksen and Balgovind 1994; Ummenhofer et al. 2008), precipitation across southern and western regions of Australia seems to be modulated by the meridional gradient in SST across the eastern Indian Ocean. We explore this further for the May–September months in the AGCM experiments, which include a range of eastern Indian Ocean SST gradients. The gradient is taken as the difference between spatially averaged SST anomalies across the P_{el} location minus SST anomalies at P_{sl} (see dashed boxes in Fig. 1). In Fig. 5, the rainfall anomalies in the AGCM ensembles for WA and SEA are shown as a function of the SST gradient that exists in the various experiments. For WA precipitation, an overall trend pattern is apparent, with negative (positive) SST gradients coinciding with drier (wetter) conditions (Fig. 5a). The P_{el} experiments have an SST gradient of $\pm 0.25^\circ\text{C}$. This translates to a significant change in precipitation relative to the CNTRL, with a median anomaly of -2.1 and $+2.7$ mm month^{-1} for the dry and wet cases, respectively. In both cases, approximately 75% of the rainfall anomalies across the ensemble members lie below/above zero, respectively.

For the P_{sl} case, the SST gradient is of a similar magnitude to that in P_{el} , but no significant shift in the rainfall distribution is found. This is most likely a result of reduced air–sea coupling in the extratropics, relative to the eastern tropical pole. This lack of a significant rainfall response over Australia is in line with earlier work that suggested that the central Indian SST anomalies are of minor importance (Frederiksen and Balgovind 1994). However, the importance of SST anomalies in the mid-latitudes should not be underestimated. When employing

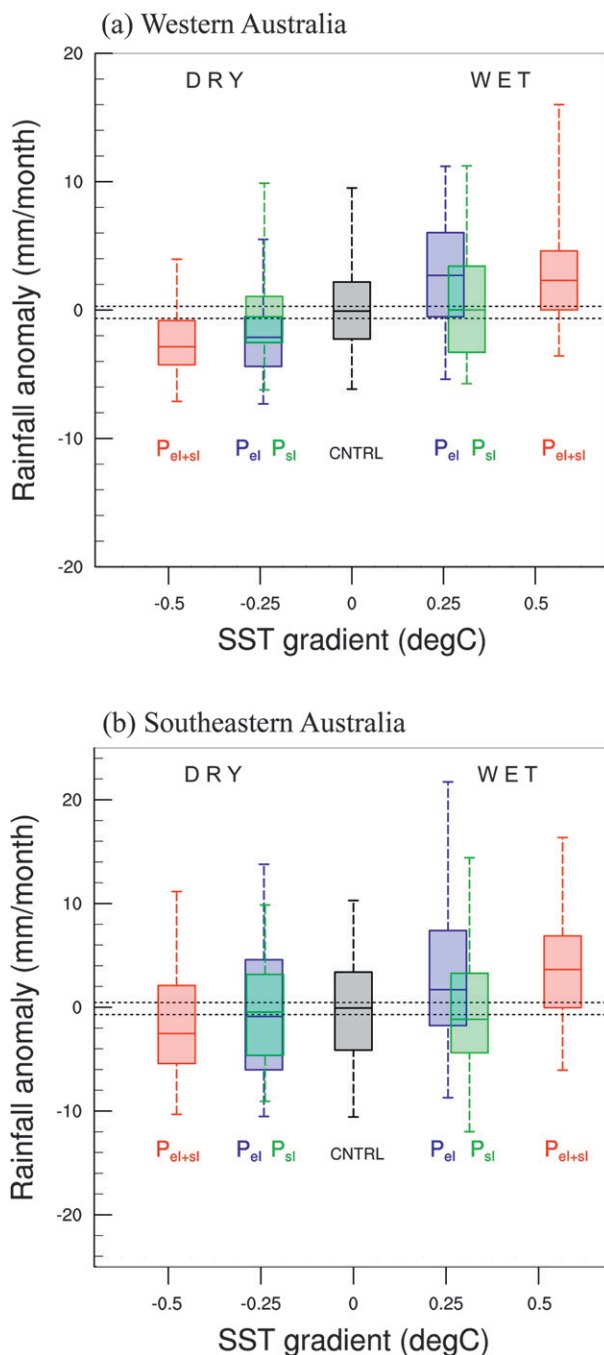


FIG. 5. Rainfall anomalies (in mm month^{-1}) plotted as a function of the SST gradient (in $^\circ\text{C}$) in the different cases averaged over the May–September months for (a) WA and (b) SEA. The colored boxes are delimited by the upper and lower quartiles, with the middle bar denoting the median rainfall. Horizontal dashed lines indicate the 90% confidence level (as estimated by Monte Carlo testing) for the medians for the different categories (indicated in color).

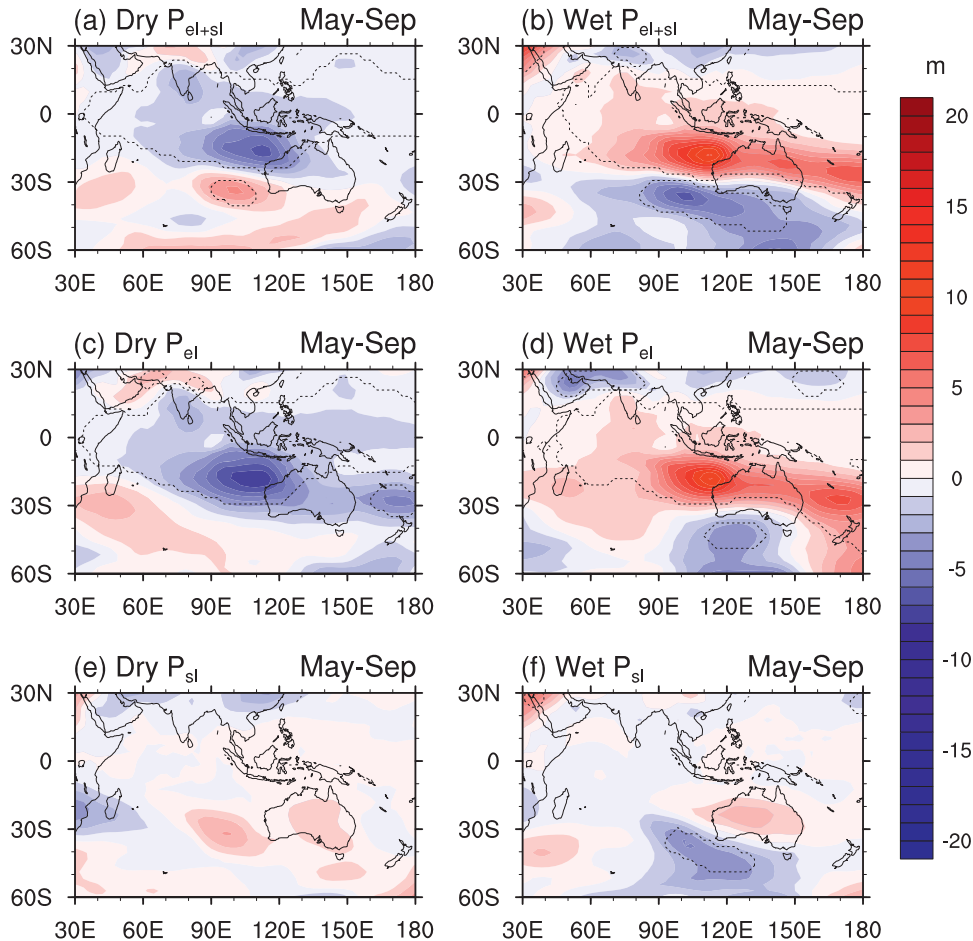


FIG. 6. Thickness anomalies (in m) for 1000–500 hPa for the (left) dry and (right) wet cases, respectively, for (a),(b) P_{el+sl} , (c),(d) P_{el} , and (e),(f) P_{sl} , averaged over the May–September months. The area enclosed by the dashed contours denotes anomalies that are significant at the 90% confidence level as estimated by a two-tailed t test.

SST anomalies there in conjunction with the tropical pole, an enhancement of the precipitation response over Australia is apparent (cf. Fig. 2). The experiments with the most extreme SST gradients (i.e., P_{el+sl} with a gradient of -0.4° and $+0.6^{\circ}\text{C}$ for the dry and wet cases, respectively) show the largest rainfall anomalies of all experiments (Fig. 5a). The median rainfall is -2.9 and $+2.3$ mm month^{-1} , respectively, which is significantly different from the CNTRL at the 90% confidence level. The changes in precipitation in relation to the SST gradient become more apparent at the extremes of the distribution. The maximum (minimum) precipitation anomaly reached in the wet case of P_{el+sl} is $+16.4$ mm month^{-1} (-6.1 mm month^{-1}), while the dry case records $+11.1$ mm month^{-1} (-10.3 mm month^{-1}). This also highlights an asymmetry between the dry and wet experiments, with the range of maximum to minimum anomalies in the dry cases generally smaller than that in the wet case. The wet

ensemble set shows a disproportionate gain of members at the upper end of the distribution, also reflected in changes in the skewness of the precipitation anomalies. This is in agreement with earlier AGCM studies that showed that the atmospheric response is more sensitive to warm than cold SST anomalies (e.g., Reason 2002; Ummenhofer et al. 2008, 2009b).

When assessing the SEA rainfall anomalies in relation to the SST gradient across the eastern Indian Ocean (Fig. 5b), we find similar patterns to WA precipitation. Anomalous dry (wet) conditions over SEA dominate across the ensemble members in the experiments with a negative (positive) SST gradient, with the rainfall anomaly being proportional to the magnitude of the SST gradient. As for WA, the P_{sl} case does not show a significant response for the dry simulation, despite a comparable SST gradient to the P_{el} case. For the P_{sl} wet case, a marginally significant median negative

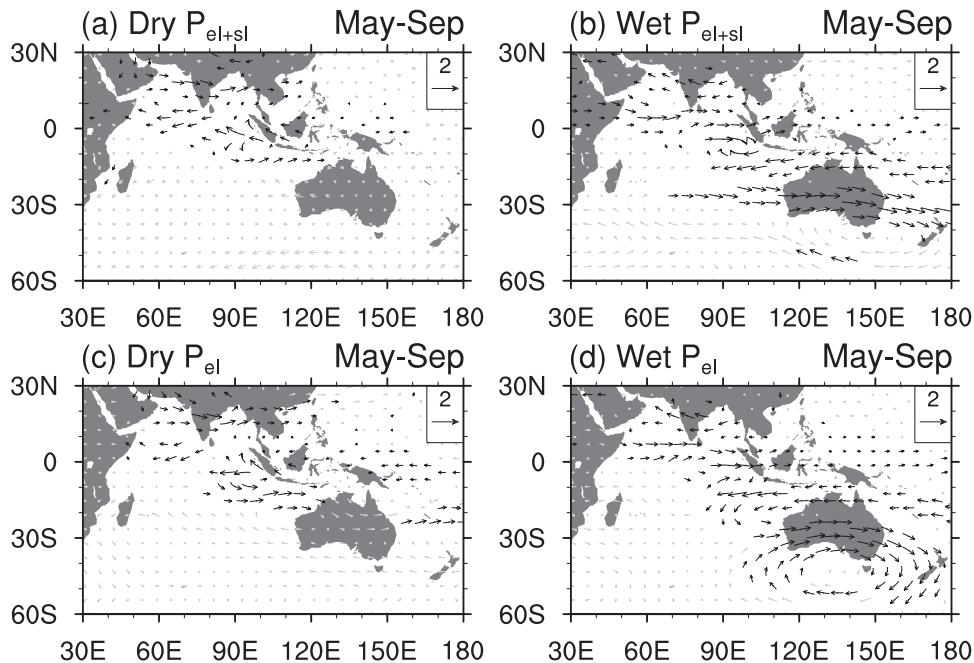


FIG. 7. Wind anomalies (in m s^{-1}) at the 500-hPa level for the (left) dry and (right) wet cases, respectively, for (a),(b) P_{el+sl} , and (c),(d) P_{el} , averaged over the May–September months. Black vectors denote anomalies that are significant at the 90% confidence level as estimated by a two-tailed t test.

rainfall anomaly is seen. Apart from this, the rainfall distribution seems to be broadly linear with respect to the sign of the gradient. The P_{el+sl} simulations with strongly reduced (enhanced) meridional SST gradients show median rainfall anomalies of $-2.5 \text{ mm month}^{-1}$ ($+3.6 \text{ mm month}^{-1}$) for the dry (wet) case. These results again indicate the predominant role of the eastern tropical pole for SEA rainfall in the AGCM simulations. However, there is also a suggestion that the southern pole with opposite polarity enhances the rainfall response, when occurring in conjunction with the eastern pole.

4. Atmospheric circulation changes

To explore the mechanisms responsible for the shifts in the rainfall distribution recorded for WA and SEA, we assess May–September anomaly fields of climate variables in the various experiments (Figs. 6–8).

The atmospheric response to the underlying SST perturbation is apparent in the thickness anomaly (1000–500 hPa) fields for the different experiments (Fig. 6). Due to ocean–atmosphere thermal coupling in the lower troposphere, thickness anomalies develop over the position of, and with the same sign as, the underlying SST anomalies. In particular, in the dry (wet) P_{el+sl} case, negative (positive) thickness anomalies occur over the cold (warm) eastern pole, while anomalies of the opposite sign are seen over the warm (cold) pole in the

subtropical Indian Ocean (Figs. 6a,b). The atmospheric anomalies extend eastward onto the adjacent Australian continent, especially in the wet case. The anomalous pattern represents a reduction (increase) in the meridional thickness gradient across the eastern Indian Ocean, consistent with a dampening (intensification) of the seasonal cycle (Ummenhofer et al. 2008). In the P_{el} case, anomalous cold (warm) SST leads to negative (positive) thickness anomalies on the order of $\pm 10 \text{ m}$ over the eastern Indian Ocean, extending over the northwest (northern half) of Australia in the dry (wet) case (Figs. 6c,d). For P_{sl} , no significant thickness anomalies occur in the dry case, while moderate negative anomalies up to -3 m appear to the southwest of Australia in the wet simulations (Figs. 6e,f). The majority of the response in the thickness anomalies in the P_{el+sl} cases seems to be due to forcing by the tropical eastern pole. However, the southern pole acts to reinforce the thickness gradient anomaly, especially for the wet case. Overall, the extent of the thickness anomalies over Australia is larger in the wet than the dry cases. This is in line with the disproportionately larger shifts recorded in the rainfall distribution in the former. The thickness anomalies with an enhanced meridional gradient across Australia in the wet P_{el+sl} and P_{el} cases are similar to those described during negative IOD events co-occurring with La Niña by Risbey et al. (2009). As described earlier, the location of the eastern pole here approximates the eastern region used by Saji

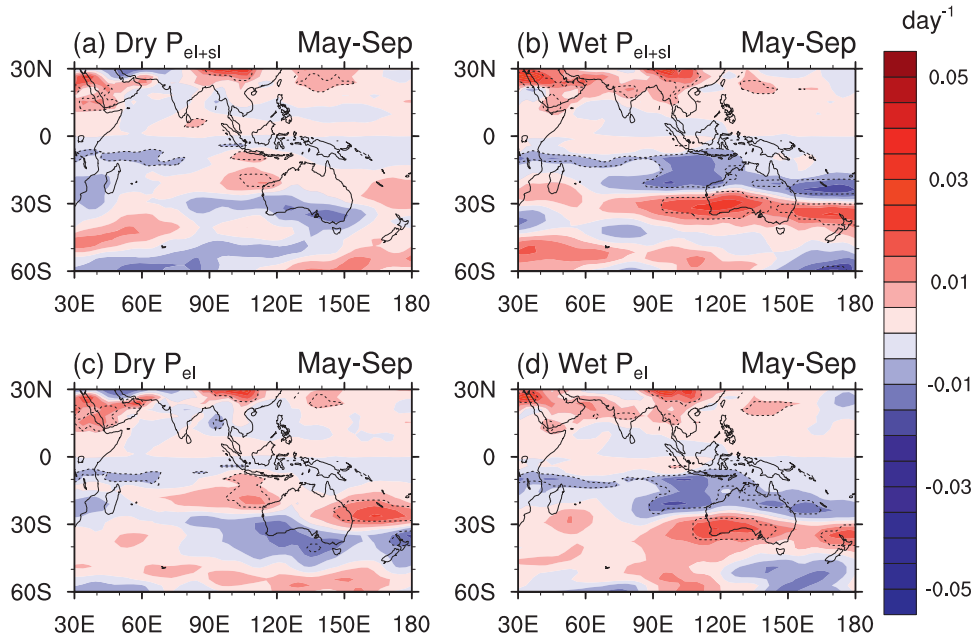


FIG. 8. Eady growth rate anomalies (in day^{-1}) for the (left) dry and (right) wet cases, respectively, for (a),(b) P_{el+sl} , and (c),(d) P_{el} , averaged over the May–September months. The area enclosed by the dashed contours denotes anomalies that are significant at the 90% confidence level as estimated by a two-tailed t test.

et al. (1999) to define the IOD index. From the experiments conducted here, and the apparent dominant role of the eastern pole, it might be hypothesized that the occurrence of the negative IOD event is a major driver in the formation of the thickness anomaly described by Risbey et al. (2009). Consequently, the same would then in turn apply for the coincident anomalous wet conditions over southern regions of Australia (Ummenhofer et al. 2009a).

The changes in the meridional thickness gradient induce anomalies in the thermal wind, shown for the 500-hPa level in Fig. 7 for the different experiments. As the P_{sl} cases do not show significant anomalies, for the remainder of the study we only present the P_{el+sl} and P_{el} cases. Significant wind anomalies for the dry P_{el+sl} case are limited to the tropics (Fig. 7a). In contrast, the wet simulation shows enhanced westerly flow over Australia south of 20°S , while anomalous easterly flow occurs across the northern tip of Australia and the eastern tropical Indian Ocean (Fig. 7b). Very similar circulation patterns are seen for the P_{el} cases (Figs. 7c,d). The wind anomalies in the wet cases (Figs. 7b,d) are indicative of an enhanced onshore moisture flux in the seasonally strengthening westerly jet, consistent with the significant increases in rainfall over WA and SEA (Figs. 2–4). Circulation anomalies in the lower atmosphere at the 850-hPa level (figure not shown) depict qualitatively similar results. For the wet P_{el+sl} case, the wind anomalies at 850 hPa closely resemble enhanced moisture flux

anomalies toward SEA during negative IOD years (Ummenhofer et al. 2009a). Similarly, in their wet case AGCM simulations, Frederiksen and Balgovind (1994) found increased cross-equatorial flow and a strong baroclinic zone across Australia, transporting warm humid air poleward, thus accounting for the anomalous wet conditions. In observations for the cool season, Risbey et al. (2009) associated wet conditions across southern regions of Australia with an equatorward shift of the zonal westerlies and enhanced frontal rainfall.

As a further diagnostic to explore the modeled precipitation changes, we present anomalies in the Eady growth rate (Fig. 8). This provides an indication of baroclinic instabilities in the atmosphere and uses the vertical gradient in horizontal wind speed and the Brunt–Väisälä frequency as a measure of static stability (Paciorek et al. 2002). Risbey et al. (2009) described a pronounced maximum in the Eady growth rate over southeastern Australia during negative IOD years, contributing to the anomalous wet conditions seen over the region during these years (Ummenhofer et al. 2009a). In the dry simulations, significant anomalies are limited to the tropics, with enhanced instabilities developing over the location of the eastern pole for the P_{el+sl} and P_{el} cases (Figs. 8a,c). The wet cases show extensive positive (negative) Eady growth rate anomalies over the southern (northern) half of Australia and across the eastern Indian Ocean (Figs. 8b,d). The increase in baroclinic instabilities over

TABLE 1. Summary of the statistical relationship between observed SST anomalies at the location of the poles (see boxes in Fig. 1) and precipitation for WA and SEA for the May–September months, using available climatologies (HadISST and Bureau of Meteorology data for rainfall) for the period 1970–2005. Correlation coefficients significant at the 90% level are highlighted in boldface.

Region	Experiment	Correlation coefficient	<i>P</i> value
WA	P_{eI}	0.47	0.004
	P_{sI}	0.28	0.097
	$P_{eI} - P_{sI}$	0.47	0.004
SEA	P_{eI}	0.43	0.009
	P_{sI}	0.09	0.596
	$P_{eI} - P_{sI}$	0.32	0.058

southern regions of Australia, including WA and SEA, could thus account for the enhanced rainfall seen there for the wet P_{eI+sI} and P_{eI} cases. Over southern regions of Australia, Frederiksen and Frederiksen (1996) described similarly enhanced baroclinicity and a northward shift of storm-track instability modes, coinciding with a strengthened meridional SST gradient across the eastern Indian Ocean, resembling the SST gradient used in the wet experiments here. Under an SST pattern resembling our wet year experiments, Drosowsky (1993b) found conditions to be favorable for an amplification of synoptic-scale disturbances over WA.

5. Observations

The results from the AGCM experiments suggest the importance of the meridional SST gradient across the eastern Indian Ocean in modulating regional Australian rainfall. It is thus of interest to compare the model results with observations. Table 1 details the relationship between SST anomalies in the various eastern Indian Ocean regions (P_{eI} , P_{sI} , and their difference) and precipitation anomalies observed for WA and SEA for the May–September months during the period 1970–2005. We find a significant positive relationship between SST anomalies in the P_{eI} and precipitation across WA and SEA at the 95% and 90% confidence levels, respectively. In contrast, the negative correlation between precipitation in both regions and SST in the central subtropical Indian Ocean (P_{sI}) is not significant at the 90% level. When combining anomalies in the two poles thereby giving the SST gradient across the eastern Indian Ocean (P_{eI+sI}), the relationship to rainfall in WA remains robust, while being slightly reduced for SEA (Table 1). This “test” of the relationship between observed precipitation and eastern Indian Ocean SST anomalies is by no means conclusive, with only approximately 30 yr of reliable Indian Ocean SST data

for the postsatellite era. However, it provides evidence that the relationships explored in the model in this study match the observations. This is in line with other observational evidence (e.g., Drosowsky 1993b; Frederiksen and Balgovind 1994).

Significant changes in Indian Ocean surface properties have been observed over the past few decades (e.g., Alory et al. 2007; Abram et al. 2008; Ihara et al. 2008). An intensification of IOD events (Abram et al. 2008) and unequal warming of the Indian Ocean over recent decades (Ihara et al. 2008) predispose the Indian Ocean to more positive IOD events. Alory et al. (2007) described subsurface cooling in the tropical eastern Indian Ocean and warming in the subtropics centered around 40°S. These recent trends in Indian Ocean properties represent a general tendency toward a reduced meridional SST gradient across the eastern Indian Ocean, which we have shown here to be associated with drier conditions across western and southern regions of Australia. Similarly for SWWA, England et al. (2006) found Indian Ocean SST to trend toward the pattern linked to below-average rainfall over the region.

6. Summary and conclusions

In this study, we have explored the role of meridional SST gradients in the eastern Indian Ocean in modulating Australian precipitation. In ensemble AGCM simulations, we quantitatively assessed the Australian rainfall response to the sign and magnitude of the meridional SST gradients between characteristic poles of enhanced variability. The study focused on the cool season rainfall response over Western Australia (WA) and southeastern Australia (SEA), two regions that have sustained significant precipitation decreases over recent decades. In general, a linear relationship is found between the *sign* of these meridional SST gradients and WA and SEA rainfall. An enhanced (reduced) SST gradient induces an increase (decrease) in the meridional atmospheric thickness gradient. This leads to an anomalous easterly (westerly) thermal wind response across Australia, accounting for the drier (wetter) conditions in the simulations (Ummenhofer et al. 2008). The response to the enhanced meridional SST gradient leading to the anomalously wet conditions is particularly prominent at the upper end of the precipitation frequency distribution. SEA rainfall responds more strongly to the forcing that brings about wet conditions compared to those associated with dry conditions, while the response for WA shows greater symmetry. Based on observations, Drosowsky (1993b) found similar results for composites of wet years relative to dry years. He suggested this was due to a weaker feedback between

the atmospheric circulation and the SST pattern in the dry phase, when the SST anomalies acted to reduce the SST gradient, suppressing development of synoptic-scale disturbances over the eastern Indian Ocean and western regions of Australia. Here we also find a disproportionately large response in the wet case, with the signal from the warm SST anomalies penetrating higher into the atmosphere, as the more unstable air column has the ability to mix the anomalies to a greater height. In contrast, the response from cold underlying SST anomalies does not extend as high into the atmosphere (Ummenhofer et al. 2008).

When decomposing the SST anomalies across the eastern Indian Ocean into their constituent “poles,” we find that in addition to the sign and *magnitude* of the gradient, the location of the forcing has a bearing on the rainfall response. By examining both Figs. 2 and 4, there appears to be a broadly linear relationship between the meridional SST gradient and rainfall for SEA wet cases, although this is less clear for WA. For WA rainfall, the eastern tropical pole SST anomalies seem to have a disproportionately large effect, with subtropical SST anomalies (of opposite sign) playing a minor role. Our experiments suggest that for both WA and SEA the southern subtropical pole on its own does not lead to a significant rainfall response. The experiments do however show that the southern pole enhances the rainfall response over SEA when the eastern pole is active. These model results broadly support the limited observational record available for the period 1970–2005 (presatellite era data are less reliable), and are in line with earlier observational work on SST gradients across the eastern Indian Ocean/Indonesian region (e.g., Nicholls 1989; Drosowsky 1993b; Frederiksen and Balgovind 1994). Recent changes in surface Indian Ocean properties (e.g., Abram et al. 2008; Ihara et al. 2008; Cai et al. 2009) highlight the need for improved understanding of the response of interannual rainfall variability to changes in SST gradients across the region. Furthermore, sustained changes in Indian Ocean SST could have profound implications for long-term rainfall trends over southern Australia.

Acknowledgments. Use of NCAR’s CCSM3 model is gratefully acknowledged. The model simulations were run at the Australian Partnership for Advanced Computing National Facility. NOAA_ERSST_V2 SST data were provided by NOAA/OAR/ESRL PSD (United States), HadISST by the Met Office, and the precipitation data are from the Australian Bureau of Meteorology. Three anonymous reviewers provided comments that helped to improve the original manuscript. This work was supported by the Australian Research Council.

REFERENCES

- Abram, N. J., M. K. Gagan, J. E. Cole, W. S. Hantoro, and M. Mudelsee, 2008: Recent intensification of tropical climate variability in the Indian Ocean. *Nature Geosci.*, **1**, 849–853, doi:10.1038/ngeo357.
- Allan, R. J., and M. R. Haylock, 1993: Circulation features associated with the winter rainfall decrease in Southwestern Australia. *J. Climate*, **6**, 1356–1367.
- Alory, G., S. Wijffels, and G. Meyers, 2007: Observed temperature trends in the Indian Ocean over 1960–1999 and associated mechanisms. *Geophys. Res. Lett.*, **34**, L02606, doi:10.1029/2006GL028044.
- Ashok, K., Z. Guan, and T. Yamagata, 2003: Influence of the Indian Ocean Dipole on the Australian winter rainfall. *Geophys. Res. Lett.*, **30**, 1821, doi:10.1029/2003GL017926.
- Behera, S. K., and T. Yamagata, 2001: Subtropical SST dipole events in the southern Indian Ocean. *Geophys. Res. Lett.*, **28**, 327–330.
- Black, E., J. Slingo, and K. R. Sperber, 2003: An observational study of the relationship between excessively strong short rains in coastal East Africa and Indian Ocean SST. *Mon. Wea. Rev.*, **131**, 74–94.
- Cai, W., and T. Cowan, 2006: SAM and regional rainfall in IPCC AR4 models: Can anthropogenic forcing account for southwest Western Australian winter rainfall reduction? *Geophys. Res. Lett.*, **33**, L24708, doi:10.1029/2006GL028037.
- , and —, 2008: Dynamics of late autumn rainfall reduction over southeastern Australia. *Geophys. Res. Lett.*, **35**, L09708, doi:10.1029/2008GL033727.
- , G. Shi, and Y. Li, 2005: Multidecadal fluctuations of winter rainfall over southwest Western Australia simulated in the CSIRO Mark 3 coupled model. *Geophys. Res. Lett.*, **32**, L12701, doi:10.1029/2005GL022712.
- , T. Cowan, and A. Sullivan, 2009: Recent unprecedented skewness towards positive Indian Ocean Dipole occurrences and its impact on Australian rainfall. *Geophys. Res. Lett.*, **36**, L11705, doi:10.1029/2009GL037604.
- Collins, W. D., and Coauthors, 2006: The Community Climate System Model version 3 (CCSM3). *J. Climate*, **19**, 2122–2143.
- D’Arrigo, R., and R. Wilson, 2008: El Niño and Indian Ocean influences on Indonesian drought: Implications for forecasting rainfall and crop productivity. *Int. J. Climatol.*, **28**, 611–616.
- Deser, C., A. Capotondi, R. Saravanan, and A. S. Phillips, 2006: Tropical Pacific and Atlantic climate variability in CCSM3. *J. Climate*, **19**, 2451–2481.
- Drosowsky, W., 1993a: An analysis of Australian seasonal rainfall anomalies: 1950–1987. I: Spatial patterns. *Int. J. Climatol.*, **13**, 1–30.
- , 1993b: An analysis of Australian seasonal rainfall anomalies: 1950–1987. II: Temporal variability and teleconnection patterns. *Int. J. Climatol.*, **13**, 111–149.
- , and L. E. Chambers, 2001: Near-global surface temperature anomalies as predictors of Australian seasonal rainfall. *J. Climate*, **14**, 1677–1687.
- England, M. H., C. C. Ummenhofer, and A. Santoso, 2006: Interannual rainfall extremes over southwest Western Australia linked to Indian Ocean climate variability. *J. Climate*, **19**, 1948–1969.
- Frederiksen, C. S., and R. C. Balgovind, 1994: The influence of the Indian Ocean/Indonesian SST gradient on the Australian winter rainfall and circulation in an atmospheric GCM. *Quart. J. Roy. Meteor. Soc.*, **120**, 923–952.

- , and J. S. Frederiksen, 1996: A theoretical model of Australian Northwest cloudband disturbances and Southern Hemisphere storm tracks: The role of SST anomalies. *J. Atmos. Sci.*, **53**, 1410–1432.
- , D. P. Rowell, R. C. Balgovind, and C. K. Folland, 1999: Multidecadal simulations of Australian rainfall variability: The role of SSTs. *J. Climate*, **12**, 357–379.
- Frederiksen, J. S., and C. S. Frederiksen, 2007: Interdecadal changes in Southern Hemisphere winter storm track modes. *Tellus*, **59A**, 599–617.
- Hack, J. J., J. M. Caron, S. M. Yeager, K. W. Oleson, M. M. Holland, J. E. Truesdale, and P. J. Rasch, 2006: Simulation of the global hydrological cycle in the CCSM Community Atmosphere Model version 3 (CAM3): Mean features. *J. Climate*, **19**, 2199–2221.
- Hastenrath, S., 2007: Circulation mechanisms of climate anomalies in East Africa and the equatorial Indian Ocean. *Dyn. Atmos. Oceans*, **43**, 25–35.
- Hendon, H. H., D. W. J. Thompson, and M. C. Wheeler, 2007: Australian rainfall and surface temperature variations associated with the Southern Hemisphere annular mode. *J. Climate*, **20**, 2452–2467.
- Hope, P. K., 2006: Projected future changes in synoptic systems influencing southwest Western Australia. *Climate Dyn.*, **26**, 765–780.
- Hurrell, J. W., J. J. Hack, A. S. Phillips, J. Caron, and J. Yin, 2006: The dynamical simulation of the Community Atmosphere Model version 3 (CAM3). *J. Climate*, **19**, 2162–2183.
- , —, D. Shea, J. M. Caron, and J. Rosinski, 2008: A new sea surface temperature and sea ice boundary dataset for the Community Atmosphere Model. *J. Climate*, **21**, 5145–5153.
- Ihara, C., Y. Kushnir, and M. A. Cane, 2008: Warming trend of the Indian Ocean SST and Indian Ocean Dipole from 1880 to 2004. *J. Climate*, **21**, 2035–2046.
- IOCI, 2002: Climate variability and change in south west Western Australia. Tech. Rep., Indian Ocean Climate Initiative Panel, Perth, Australia, 43 pp.
- Lavery, B., G. Joung, and N. Nicholls, 1997: An extended high-quality historical rainfall dataset for Australia. *Aust. Meteor. Mag.*, **46**, 27–38.
- Meehl, G. A., J. M. Arblaster, D. M. Lawrence, A. Seth, E. K. Schneider, B. P. Kirtman, and D. Min, 2006: Monsoon regimes in the CCSM3. *J. Climate*, **19**, 2482–2495.
- Murphy, B. F., and B. Timbal, 2008: A review of recent climate variability and climate change in southeastern Australia. *Int. J. Climatol.*, **28**, 859–879.
- Nicholls, N., 1989: Sea surface temperatures and Australian winter rainfall. *J. Climate*, **2**, 965–973.
- Paciorek, C. S., J. S. Risbey, V. Ventura, and R. D. Rosen, 2002: Multiple indices of Northern Hemisphere cyclone activity, winters 1949–99. *J. Climate*, **15**, 1573–1590.
- Pitman, A. J., G. T. Narisma, R. A. Pielke Sr., and N. J. Holbrook, 2004: Impact of land cover change on the climate of southwest Western Australia. *J. Geophys. Res.*, **109**, D18109, doi:10.1029/2003JD004347.
- Rayner, N. A., D. E. Parker, E. B. Horton, C. K. Folland, L. V. Alexander, and D. P. Rowell, 2003: Global analyses of SST, sea ice and night marine air temperature since the late nineteenth century. *J. Geophys. Res.*, **108**, 4407, doi:10.1029/2002JD002670.
- Reason, C. J. C., 2002: Sensitivity of the southern African circulation to dipole sea-surface temperature patterns in the South Indian Ocean. *Int. J. Climatol.*, **22**, 377–393.
- Risbey, J. S., M. J. Pook, P. C. McIntosh, C. C. Ummenhofer, G. Meyers, and M. J. Reeder, 2009: Variability of synoptic features associated with cool season rainfall in southeastern Australia. *Int. J. Climatol.*, **29**, 1595–1613.
- Saji, N. H., and T. Yamagata, 2003: Possible impacts of Indian Ocean dipole mode events on global climate. *Climate Res.*, **25**, 151–169.
- , B. N. Goswami, P. N. Vinayachandran, and T. Yamagata, 1999: A dipole mode in the tropical Indian Ocean. *Nature*, **401**, 360–363.
- Santoso, A., 2005: Evolution of climate anomalies and variability of Southern Ocean water masses on interannual to centennial timescales. Ph.D. thesis, University of New South Wales, 326 pp.
- Smith, T. M., and R. W. Reynolds, 2003: Extended reconstruction of global sea surface temperatures based on COADS data (1854–1997). *J. Climate*, **16**, 1495–1510.
- , and —, 2004: Improved extended reconstruction of SST (1854–1997). *J. Climate*, **17**, 2466–2477.
- Timbal, B., and J. M. Arblaster, 2006: Land cover change as an additional forcing to explain the rainfall decline in the south west of Australia. *Geophys. Res. Lett.*, **33**, L07717, doi:10.1029/2005GL025361.
- , —, and S. Power, 2006: Attribution of the late-twentieth-century rainfall decline in southwest Australia. *J. Climate*, **19**, 2046–2062.
- Ummenhofer, C. C., A. Sen Gupta, M. J. Pook, and M. H. England, 2008: Anomalous rainfall over southwest Western Australia forced by Indian Ocean sea surface temperatures. *J. Climate*, **21**, 5113–5134.
- , M. H. England, G. A. Meyers, P. C. McIntosh, M. J. Pook, J. S. Risbey, A. Sen Gupta, and A. S. Taschetto, 2009a: What causes Southeast Australia's worst droughts? *Geophys. Res. Lett.*, **36**, L04706, doi:10.1029/2008GL036801.
- , A. Sen Gupta, M. H. England, and C. J. C. Reason, 2009b: Contributions of Indian Ocean sea surface temperatures to enhanced East African rainfall. *J. Climate*, **22**, 993–1013.
- Vecchi, G. A., and B. J. Soden, 2007: Global warming and the weakening of the tropical circulation. *J. Climate*, **20**, 4316–4340.
- von Storch, H., and F. W. Zwiers, 1999: *Statistical Analysis in Climate Research*. Cambridge University Press, 484 pp.
- Webster, P. J., A. M. Moore, J. P. Loschnigg, and R. R. Leben, 1999: Coupled ocean-atmosphere dynamics in the Indian Ocean during 1997–98. *Nature*, **401**, 356–360.
- Zelle, H., G. J. van Oldenborgh, G. Burgers, and H. Dijkstra, 2005: El Niño and greenhouse warming: Results from ensemble simulations with the NCAR CCSM. *J. Climate*, **18**, 4669–4683.
- Zhang, G., and H. Wang, 2006: Toward mitigating the double ITCZ problem in NCAR CCSM3. *Geophys. Res. Lett.*, **33**, L06709, doi:10.1029/2005GL025229.